• **Basic Research** •

Multimodal imaging of experimental choroidal neovascularization

Ioanna Tsioti[1], Xuan Liu[1,2], Petra Schwarzer[1], Martin S. Zinkernagel[1], Despina Kokona[1]

[1]Department of Ophthalmology, Inselspital, Bern University Hospital, and Department of BioMedical Research, University of Bern, Bern 3010, Switzerland

[2]Department of Ophthalmology, the First Affiliated Hospital of Xi'an Jiaotong University, Xi'an 710061, Shaanxi Province, China

Co-first authors: Ioanna Tsioti and Xuan Liu

Correspondence to: Despina Kokona. Department of Ophthalmology, Inselspital, Bern University Hospital, Freiburgstrasse 4, Bern 3010, Switzerland. despina.kokona@insel.ch

Abstract

● **AIM:** To compare choroidal neovascularization (CNV) lesion measurements obtained by *in vivo* imaging modalities, with whole mount histological preparations stained with isolectin GS-IB4, using a murine laser-induced CNV model.

● **METHODS:** B6N.Cg-Tg(Csf1r-EGFP)1Hume/J heterozygous adult mice were subjected to laser-induced CNV and were monitored by fluorescein angiography (FA), multicolor (MC) fundus imaging and optical coherence tomography angiography (OCTA) at day 14 after CNV induction. Choroidal-retinal pigment epithelium (RPE) whole mounts were prepared at the end of the experiment and were stained with isolectin GS-IB4. CNV areas were measured in all different imaging modalities at day 14 after CNV from three independent raters and were compared to choroidal-RPE whole mounts. Intraclass correlation coefficient (ICC) type 2 (2-way random model) and its 95% confidence intervals (CI) were calculated to measure the correlation between different raters' measurements. Spearman's rank correlation coefficient (Spearman's *r*) was calculated for the comparison between FA, MC and OCTA data and histology data.

● **RESULTS:** FA (early and late) and MC correlates well with the CNV measurements *ex vivo* with FA having slightly better correlation than MC (FA early Spearman's *r*=0.7642, FA late Spearman's *r*=0.7097, and MC Spearman's *r*=0.7418), while the interobserver reliability was good for both techniques (FA early ICC=0.976, FA late ICC=0.964, and MC ICC=0.846). In contrast, OCTA showed a poor correlation with *ex vivo* measurements (Spearman's *r*=0.05716) and high variability between different raters (ICC=0.603).

● **CONCLUSION:** This study suggests that FA and MC imaging could be used for the evaluation of CNV areas *in vivo* while caution must be taken and comparison studies should be performed when OCTA is employed as a CNV monitoring tool in small rodents.

● **KEYWORDS:** choroidal neovascularization; *in vivo* imaging; fluorescein angiography; multicolor fundus imaging; optical coherence tomography angiography

INTRODUCTION

Exudative (wet) age-related macular degeneration (wAMD) is one of the most common retinal diseases that causes visual impairment and blindness in the elderly population[1-2]. The formation of new abnormal blood vessels beneath the retina and into the choroid is the main characteristic of the disease[3]. Laser-induced choroidal neovascularization (CNV) is used as an experimental model of AMD in rodents and it relies on the rupture of Bruch's membrane and subsequent neovascularization, similar to that seen in human AMD where new choroidal vessels migrate spontaneously into the sub-retinal pigment epithelium (RPE) or sub-retinal space[4]. This model can be utilized for the evaluation of treatment approaches as well as for the investigation of the disease pathophysiology in small animals. However, for several reasons, *in vivo* monitoring of CNV lesions overtime would be beneficial. Until today, the gold standard for CNV lesion measurements in rodents relies on histological preparations. Yet, histology requires euthanasia of the animal and cannot be used for longitudinal studies. In the clinical practice imaging modalities such as fluorescein angiography (FA), multicolor (MC) fundus imaging and optical coherence tomography angiography (OCTA), are used as diagnostic tools of retinal impairments, providing important information about the disease outcome[5].

More recently, FA and OCTA have been utilized in experimental models of retinal disease in small rodents, providing a valuable tool for the imaging of the rodent retina overtime[6-10]. FA is a semi-invasive technique that requires the systemic injection of the dye fluorescein. Approximately 80% of fluorescein is bound to blood proteins while the remaining fluorescein circulates in the bloodstream and fluoresces when excited by blue light. FA provides two-dimensional images or retinal vasculature while it has limited access to the deep retinal capillary plexus and the choroidal vasculature[11]. OCTA on the other hand, is a less invasive technique that does not require dye injection and produces high-resolution three-dimensional images of the retinal and choroidal vasculature[12-13]. OCTA detects changes in the OCT reflectance signal resulting from the flow of red blood cells (RBCs). This can lead to artifacts related to RBCs flow and to motion artifacts due to eye movements. Despite these limitations, OCTA is increasingly used in the clinics and could potentially provide more information on eye pathophysiology combined with other imaging techniques.

Another recently established imaging tool is the MC imaging of the fundus, recently developed by Heidelberg engineering (Heidelberg Engineering GmbH, Heidelberg, Germany)[14]. MC imaging uses three different wavelengths, blue (486 nm), green (518 nm) and infrared (815 nm), to provide information about the superficial retina, the vascular details of the retina and retinal pigment epithelium (RPE) and choroidal structures, respectively, providing a pseudocolor image of the retina. While MC imaging has gained interest among ophthalmologists, it has not yet been evaluated as a monitoring tool for murine CNV[14-15].

The aim of the present study is to evaluate the correlation of CNV lesion measurements between the semi or non-invasive imaging techniques FA, MC imaging and OCTA, with histological preparations of choroidal-RPE whole mounts.

MATERIALS AND METHODS

Ethical Approval All animals were treated according to the ARVO Statement for the Use of Animals in Ophthalmic and Vision Research and after government approval according to the Federal Swiss Regulation on Animal Welfare.

Animals B6N.Cg-Tg(Csf1r-EGFP)1Hume/J (MacGreen) heterozygous adult mice were used. The mice were maintained at the Department of Clinical Research, University Hospital of Bern, under conditions that are describes elsewhere[16].

Anesthesia For anesthesia, necessary for CNV induction and *in vivo* imaging, the mice were injected subcutaneously with medetomidine (1 mg/kg Dormitor 1 mg/mL; Provet AG, Lyssach, Switzerland) and ketamine (80 mg/kg Ketalar 50 mg/mL; Parke-Davis, Zurich, Switzerland). For anesthesia reversal, atipamezole (2.25 mg/kg Antisedan 5 mg/mL; Provet

AG), an antagonist of medetomidine, was administered at the earliest 30min after anesthesia.

Choroidal Neovascularization Induction Experimental CNV was induced using laser photocoagulation. A 532-nm argon laser (Visulas 532s; Carl Zeiss Meditec AG, Oberkochen, Germany) with a slit-lamp adapter (Iridex Corporation, Mountain View, CA, USA) on a slit-lamp (BM900; Haag-Streit AG, Koeniz, Switzerland) was used for the CNV induction. Pupil dilation was achieved with application of tropicamide 0.5% phenylephrine 2.5% eyedrops (Hospital Pharmacy, Inselspital, Bern, Switzerland). Three laser lesions (100ms, 300 mW, 50 μm size) were applied around the optic nerve head of each eye.

Optical Coherence Tomography Angiography OCTA was performed on a Zeiss PLEX Elite 9000 device (Carl Zeiss Meditec AG, Jena, Germany) after pupil dilation with tropicamide 0.5% phenylephrine 2.5% eyedrops. A 28 D lens (Volk Optical Inc., OH, USA) in front of PLEX Elite 9000 device with 3×3 mm^2 scanning dimension (scaled for humans) was used. The different en face OCTA images obtained included the outer retina to choriocapillaris image (ORCC), the choriocapillaris image (CC), the RPE-RPE fit image and the retina image. The images were exported as BMP files with a resolution of 1024×1024 pixels for CNV area measurements.

Multicolor Imaging Immediately after OCTA, mice were imaged using the Multicolor module of a Heidelberg Spectralis HRA 2 system (Heidelberg Engineering GmbH, Heidelberg, Germany) with a widefield 55° lens (Heidelberg Engineering GmbH, Heidelberg, Germany). Images of 768×768 pixels were acquired and exported as tagged image file format (TIF) files.

Fluorescein Angiography FA was performed after MC and immediately after the subcutaneous injection of 50 μL fluorescein (0.01%; Faure; Novartis, Switzerland), diluted in $1\times$ phosphate buffered saline (PBS). Images were acquired using the Spectralis HRA 2 system with an ultra-widefield 102° lens (Heidelberg Engineering GmbH, Heidelberg, Germany). Early phase images were acquired during the first 90s of fluorescein injection, while late phase images were acquired approximately 10min later. All images were acquired in a resolution of 1536×1536 pixels and were exported as TIF files.

Choroidal-Retinal Pigment Epithelium Whole Mounts After imaging, the mice were euthanized with CO_2 inhalation and their eyes were removed and fixed in 4% paraformaldehyde solution (PFA; pH 7.4) for 10min at room temperature. The cornea, lens and retina were removed and the choroid-RPE complex was incubated for 50min in 4% PFA (pH 7.4), followed by washing in $1\times$PBS, 0.5% TritonX-100 (Sigma-Aldrich, St. Louis, MO, USA). Tissues were incubated with isolectin GS-IB4 from Griffonia simplicifolia (Alexa Fluor 647

conjugate; 1:100; Thermo Fisher Scientific, Waltham, MA, USA) at 4ºC overnight under continuous shaking. The samples were washed in 1×PBS, four radial cuts were made and the tissues were mounted on a slide with the RPE facing up.

Microscopy Microscopy was performed on equipment provided by the Microscopy Imaging Center (MIC), University of Bern, Switzerland. An inverted Zeiss LSM 710 fluorescence confocal microscope (Carl Zeiss Meditec AG, Jena, Germany) was used for the examination of choroidal-RPE whole mounts. Tile scans (3×3) z-stacks of 100-110 μm with 5 μm intervals were obtained capturing the CNV lesions with the optic nerve positioned at the center of the image. Maximum intensity projections were created in ZEN 2.5 software (Carl Zeiss Meditec AG, Jena, Germany) and exported as TIF files.

Quantification of the Choroidal Neovascularization Areas Image J (version 1.51; http://imagej.nkh.gov by the National Institutes of Health, Bethesda, MD, USA) was used for the CNV area measurements. In images obtained from MC, FA, and OCTA CNV areas were measured in pixel since the scale bars provided by the Spectralis and the PLEX Elite system are calculated for human eyes and are not accurate in mice[17]. For choroidal-RPE whole mounts, CNV areas were measured in both pixels and mm^2. Unedited images were opened in Image J and the CNV area was delineated and measured using the polygon selection tool function.

Statistical Analysis Prism 8 (Softpad Software, Inc., La Jolla, CA, USA) and IBM SPSS Statistics 25 software (SPSS Inc., Chicago, IL) were used for the statistical analysis. CNV areas were measured by two different observers in all different modalities used. To evaluate the correlation of different observers' ratings, intraclass correlation coefficient (ICC) type 2 (2-way random model) and its 95% confidence intervals (CI) were calculated. To compare different imaging methods with histology the mean pixel values of the two observers were used. Spearman's rank correlation coefficient (Spearman's r) was calculated for the comparison between FA, MC and OCTA data and data derived from histology. $P<0.05$ were considered statistically significant.

RESULTS

Imaging of the Choroidal Neovascularization Area with Different Modalities Individual laser spots were compared using different imaging modalities (Figure 1). In choroidal-RPE whole mounts the CNV areas could be identified as isolectin GS-IB4 positive signal under the confocal microscope (Figure 1A and 1F). In MC imaging, the pseudocolor image, derived from the combination of blue, green and infrared reflectance, was used for the measurement of CNV areas (Figure 1B and 1G). For FA, an early (Figure 1C, 1H) and a late phase image (Figure 1D and 1I) was obtained per eye. Fluorescein leakage was observed in both early and late phase, while it was more

pronounced in the late phase. In OCTA, CNV areas were measured in the RPE-RPE fit image (Figure 1E and 1J) based on previous studies[18]. In all imaging modalities, CNV areas were delineated manually by two independent observers, as shown in Figure 1, and were measured with the image J software.

Images Acquired with Optical Coherence Tomography Angiography and Multicolor Fundus Imaging Four OCTA en face images were exported, generated from four different slabs. The outer retina to choriocapillaris (ORCC) image (Figure 2A), the choriocapillaris (CC) image (Figure 2B), the RPE-RPE fit image (Figure 2C) and the retina image (Figure 2D). The area of CNV lesions appeared hyporeflective in the ORCC image. In CC and RPE-RPE fit images CNV areas were detected as hyperreflective, while in the retina image neovascularization was barely detectable. A dark ring surrounding the CNV area was seen in the RPE-RPE fit images (Figure 2C) and the CNV areas were measured inside this ring. In MC images, blue and green reflectance images, corresponding to the inner retina and vitreoretinal interface, and retinal vascular details in humans, appeared identical (Figure 2E and 2F). In the infrared image, corresponding to RPE and choroidal structures, CNV areas were clearly seen and were surrounded by a hyperreflective ring (Figure 2G). The pseudocolor image obtained from the combination of blue, green and infrared reflectance images was used for the analysis and the CNV area was measured as the area inside the hyperreflective ring (Figure 2H).

Interobserver Agreement The interobserver reliability was assessed by calculating the ICC and CI and by constructing Bland-Altman plots. The interobserver reliability was excellent for FA early (ICC=0.976) and FA late (ICC=0.964), good for whole mounts (ICC=0.896) and MC imaging (ICC=0.846) and moderate for OCTA (ICC=0.603; Figure 3A-3E and Table 1). Bland-Altman plots for whole mounts, FA early and OCTA are depicted in Figure 3F-3H and the values obtained from the analysis are shown in Table 2.

Correlation Between Different Imaging Modalities and Whole Mount Preparations The agreement between the measurements obtained by different imaging modalities and choroidal-RPE whole mounts was evaluated by calculation of Spearman's correlation (Table 3) and construction of Bland-Altman plots (Figure 4A-4D; Table 4). Mean CNV area measured on the whole mounts was better correlated with areas measured in the FA early (Spearman's r=0.7642), while FA late and MC showed a moderate correlation (Spearman's r=0.7097 and 0.7418, respectively) with whole mounts. OCTA correlated poorly with whole mount measurements, having a Spearman's r of 0.05716 (Table 3). Bland-Altman plots of the best (FA early) and the worst (OCTA) correlated modalities are presented in Figure 4E, 4F. For better comparison of the data
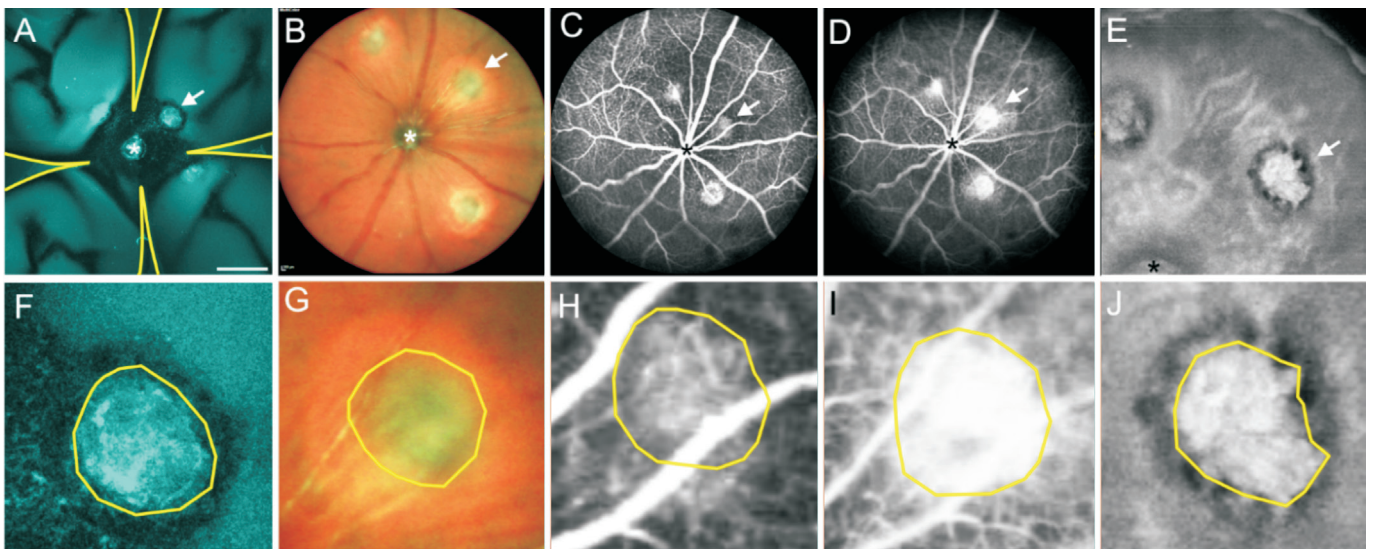
Figure 1 Imaging of the CNV area with different modalities in mice　A: Choroidal-RPE whole mounts stained with isolectin GS-IB4. Four radial cuts are delineated; B: Pseudocolor image of the retina captured with the MC imaging tool of the Spectralis system; C: Early phase FA obtained at maximum 90s after fluorescein injection; D: Late phase FA obtained approximately 10min after fluorescein injection; E: En face OCTA RPE-RPE fit image used for CNV area measurements. Magnifications of the CNV lesion indicated by arrows in A, B, C, D, and E are depicted in F, G, H, I, and J, respectively. Arrows: The same CNV lesion imaged with different modalities and measured as shown in the magnified images; Delineations: The area measured; Asterisks: Optic nerve head; Scale bar in A: 500 µm. CNV: Choroidal neovascularization; MC: Multicolor fundus imaging; FA: Fluorescein angiography; OCTA: Optical coherence tomography angiography.
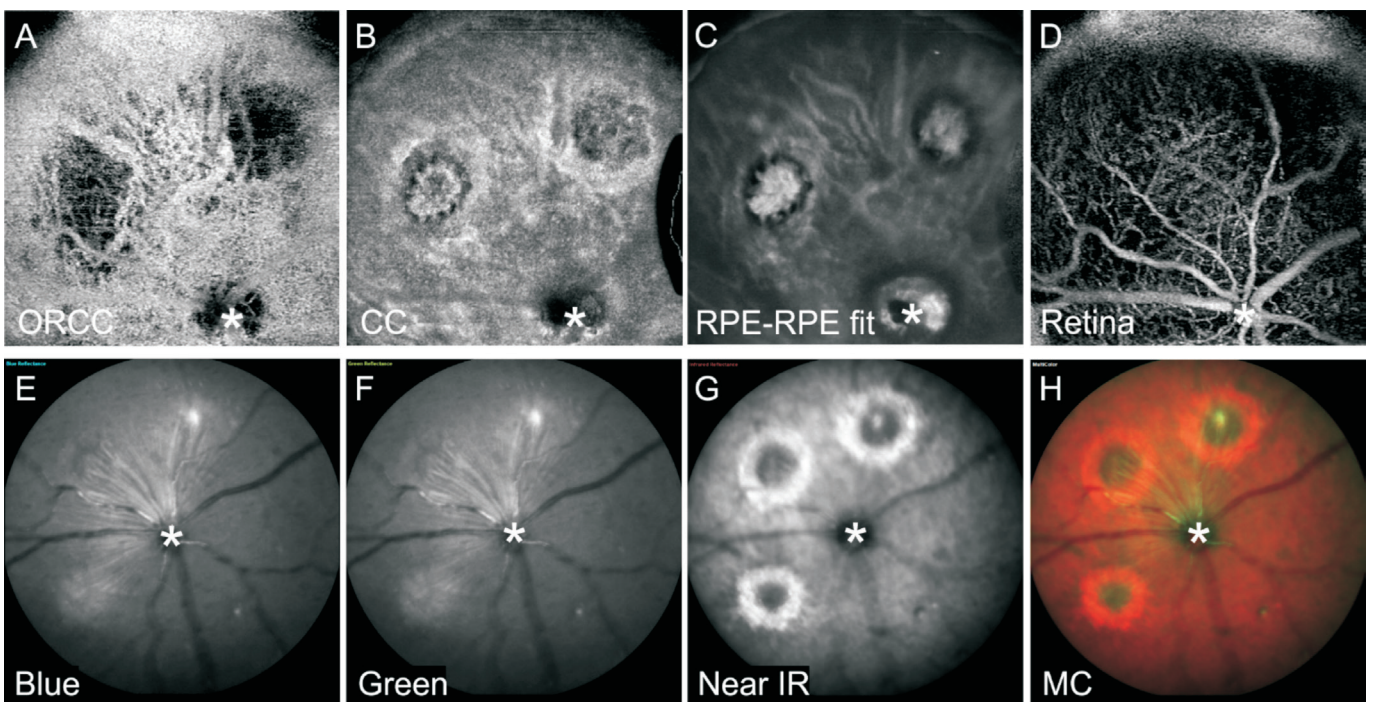

Figure 2 Images obtained by OCTA and MC imaging　Representative en face OCTA ORCC (A), CC (B), RPE-RPE fit (C), and retina (D) images obtained from a single eye. Blue (E), green (F), and infrared reflectance (G) images derived from MC imaging of a single eye. The pseudocolor image used for the CNV lesion measurements is also shown (H). RPE: Retinal pigment epithelium; Asterisk: Optic nerve head; CNV: Choroidal neovascularization; OCTA: Optical coherence tomography angiography; ORCC: Outer retina to choriocapillaris; CC: Choriocapillaris; RPE: Retinal pigment epithelium; IR: Infrared radiation; MC: Multicolor fundus imaging.

obtained by different modalities, pixel measurements of CNV area in whole mounts were used for the construction of Bland-Altman plots.

DISCUSSION
In experimental ophthalmology, histology remains the gold standard for investigation of retinal pathology. However, the
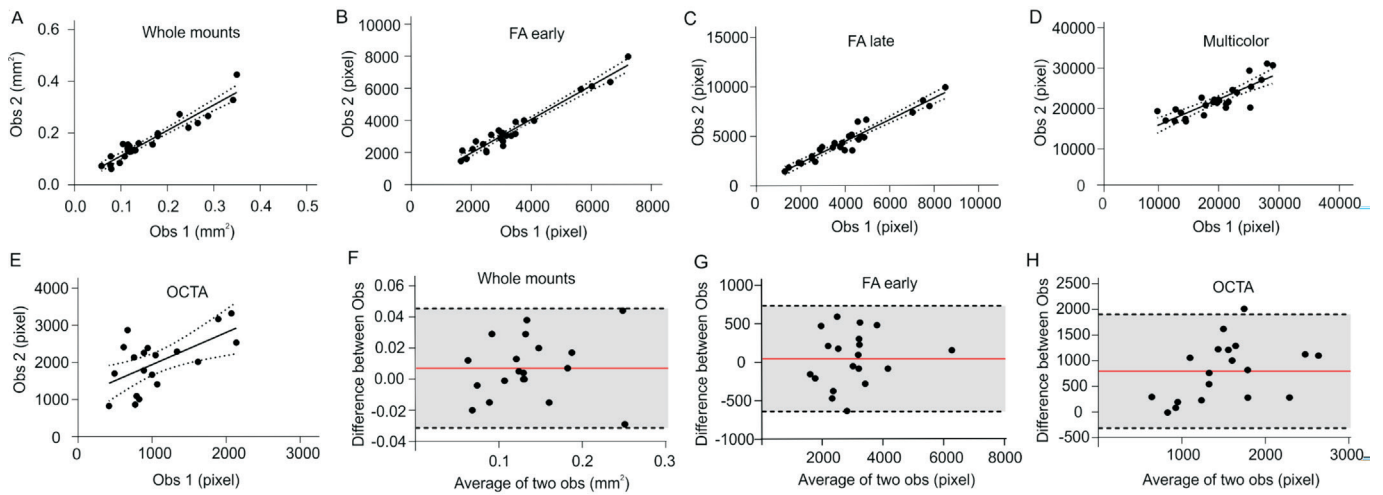
Figure 3 Correlation graphs and Bland-Altman plots of different measurements between two independent observers A: Correlation graph of whole mount measurements; B: Correlation graph of FA early measurements; C: Correlation graph of FA late measurements; D: Correlation graph of multicolor measurements; E: Correlation graph of OCTA measurements. F-H: Bland-Altman plots for the intraobserver agreement of whole mount, FA early, and OCTA measurements, respectively. Solid line in F, G, H: The mean difference between the two observers; Dotted lines: 95% confidence intervals (A, B, C, D, E) or 95% upper and lower limits of agreement (F, G, H). FA: Fluorescein angiography; OCTA: Optical coherence tomography angiography.
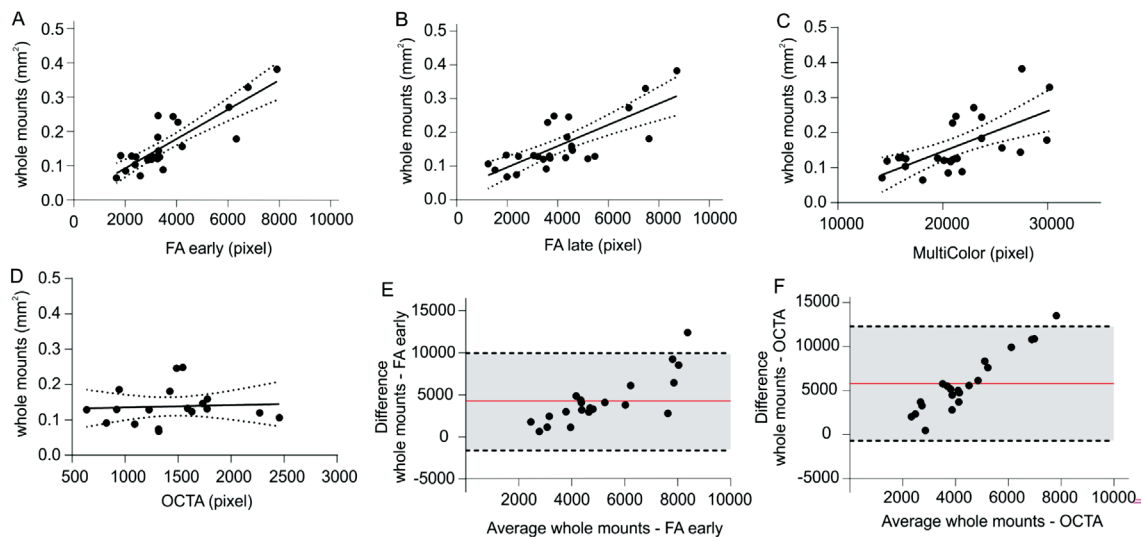

Figure 4 Correlation graphs and Bland-Altman plots of different measurements between different imaging modalities Correlation graphs of whole mount measurements *vs* FA early measurements (A), FA late measurements (B), multicolor measurements (C) and OCTA measurements (D). Bland-Altman plots for the agreement between whole mount and FA early measurements (E) and whole mount and OCTA measurements (F). Solid line in E, F: Mean difference between the two methods; Dotted lines: 95% confidence intervals (A, B, C, D) or 95% upper and lower limits of agreement (E, F). FA: Fluorescein angiography; OCTA: Optical coherence tomography angiography.

many disadvantages associated with histology have led to the utilization of imaging techniques that can provide information about retinal pathophysiology *in vivo* and in a longitudinal manner. In the present study, we evaluated the agreement of different *in vivo* imaging modalities, namely FA, MC imaging and OCTA, with histological preparations, to measure CNV areas in a murine laser-induced CNV model. The presented data generally revealed high interobserver agreement in the measurements obtained by different modalities. However, when different *in vivo* imaging modalities were compared to

measurements on choroidal-RPE whole mounts, FA and MC showed a good agreement while OCTA was poorly correlated with whole mount measurements.

To date, FA along with indocyanine green angiography (ICGA) and spectral domain optical coherence tomography, represent the standard tools for the detection of vascular abnormalities in human retina and choroid[19-22]. FA is an semi-invasive technique, since it requires systemic injection of the dye fluorescein, and despite its ability to focus in the superficial retinal vasculature, it has limited access to the visualization of

Table 1 Calculation of ICC between different observers

Obs 1 *vs* Obs 2	ICC	95%CI	Significance
Whole mounts	0.896	0.791-0.950	*P*<0.0001
FA early	0.976	0.949-0.989	*P*<0.0001
FA late	0.964	0.925-0.983	*P*<0.0001
MC	0.846	0.698-0.924	*P*<0.0001
OCTA	0.603	0.253-0.814	*P*<0.001

ICC: Intraclass correlation coefficient; Obs: Observer; 95%CI: 95% confidence interval; FA: Fluorescein angiography; MC: Multicolor fundus imaging; OCTA: Optical coherence tomography angiography.

Table 2 Statistics obtained from Bland-Altman analysis of different observers' measurements

Parameters	Bias	SD of bias	Lower LoA	Upper LoA
Whole mounts	0.007053	0.01960	-0.03137	0.04547
FA early	51.90	366.8	-667.1	770.9
FA late	472.4	516.9	-540.8	1486
MC	2690	2004	-1238	6618
OCTA	808.1	554.9	-279.6	1896

Bias: Mean difference between two observers; SD: Standard deviation; LoA: Limits of agreement; FA: Fluorescein angiography; MC: Multicolor fundus imaging; OCTA: Optical coherence tomography angiography.

Table 3 Calculation of Spearman's *r* between different methods

Whole mounts	Spearman's *r*	95%CI	Significance
FA early	0.7642	0.5389-0.8875	*P*<0.0001
FA late	0.7097	0.4487-0.8592	*P*<0.0001
MC	0.7418	0.5011-0.8759	*P*<0.0001
OCTA	0.05716	-0.3956-0.4876	*P*>0.05

Spearman's *r* was calculated to compare the agreement of CNV area measurements in the *in vivo* imaging modalities with measurements in choroidal-RPE whole mounts. FA: Fluorescein angiography; MC: Multicolor fundus imaging; OCTA: Optical coherence tomography angiography.

Table 4 Statistics obtained from Bland-Altman analysis of different methods

Whole mounts	Bias	SD of Bias	Lower LoA	Upper LoA
FA early	4269	2899	-1413	9952
FA late	3819	2915	-1893	9532
MC	13432	4515	4582	22281
OCTA	5804	3314	-691.8	12299

Comparison of CNV area measurements in *in vivo* imaging modalities and choroidal-RPE whole mounts. SD: Standard deviation; LoA: Limits of agreement; FA: Fluorescein angiography; MC: Multicolor fundus imaging; OCTA: Optical coherence tomography angiography; RPE: Retinal pigment epithelium.

deep capillary structures[23]. This weakness can be overcome by the recent development of OCTA, which is a non-invasive and more efficient tool for the imaging of retinal and choroidal vasculature based on blood flow[12,24]. OCTA is widely used in clinical ophthalmology as a tool for the study of vascular pathology in many retinal diseases and it has been recently used as an imaging tool of retinal vasculature in naïve mice and mice subjected to laser-induced CNV, using an RTVue XR Avanti system (Optovue, Inc., Fremont, California)[25]. However, previous studies have shown a lack of sensitivity and specificity of OCTA compared to FA imaging modality to detect CNV, while such comparisons with histological preparations is missing.

Since OCTA requires repeated scans of the same location in the eye in order to detect blood flow, eye movements can increase noise and lead to motion artifacts and overestimation of the blood flow signal. Moreover, projections artifacts from vessels in the superficial retina that can be seen in the deeper retina and vice versa can prevent the recognition of CNV or can inaccurately recognize the presence of CNV[26-27]. As shown in Figure 2A, the location of CNV lesions appeared hyporeflective in the ORCC images, most probably due to this kind of projection artifacts. The above mentioned limitations of OCTA along with the poor correlation of our CNV measurements in OCTA with CNV measurements in histological preparations, indicate that the Zeiss PLEX Elite 9000 OCTA system cannot be used as a reliable method for CNV measurements in mice.

Another imaging modality extensively used in the clinical practice is the MC imaging system. MC uses lasers of different colors at the same time to capture information from different retinal structures creating a high-contrast pseudocolor image of the retina. A recent study by Muftuoglu *et al*[28] reported differences in MC imaging compared to color fundus photography in patients with choroidal and/or retinal lesions. While the same information could be obtained by the two methods, MC imaging underestimated the size of choroidal lesions by 33%[28]. In our study, imaging modalities designed for humans were used for the measurement of CNV areas in mice. Thus, we were unable to use the scale bars provided by the different imaging modalities for the precise estimation of CNV size. CNV areas were clearly seen in the infrared image derived from MC imaging. All CNV lesions were surrounded by a hypperreflective ring, similar to the hyporeflective ring surrounding CNV lesions in OCTA (Figure 3A). We speculate that this ring most probably corresponds to blood, drusen, exudates or retinal atrophy in the area adjacent to the laser spot (Figure 2G), since infrared reflectance predominantly visualizes outer retina/choroidal structures[29-30].

To summarize, the present study shows that FA and MC imaging, but not OCTA performed on the Zeiss PLEX Elite 9000 device, correlate well with histological CNV measurements in isolectin GS-IB4-stained choroidal-RPE

whole mounts and therefore FA and MC may be better suited for longitudinal monitoring of CNV lesions in mice. However, caution must be taken when utilizing imaging modalities designed for humans in small rodents. Most importantly, since the mouse eye dimensions and curvature greatly differ from human eyes and the scale bars in the imaging modalities used in the present study are not accurate in small rodents, measurements and comparisons of the CNV areas were done in pixel. Thus, the comparisons were made on the proportional size of CNV rather than the actual size.

REFERENCES

1 Ma HH, Liutkevičienė R. Age-related macular degeneration: what do we know so far? *Acta Med Litu* 2021;28(1):36-47.

2 Okonkwo ON, Ibanga A, Adenuga O, Nkanga D, Ovienra W, Agweye CT, Akanbi T, Oyekunle I, Udoh MM. Burden and presentation of age-related macular degeneration among nigerians. *Middle East Afr J Ophthalmol* 2021;28(2):87-92.

3 Ambati J, Ambati BK, Yoo SH, Ianchulev S, Adamis AP. Age-related macular degeneration: etiology, pathogenesis, and therapeutic strategies. *Surv Ophthalmol* 2003;48(3):257-293.

4 Zhao M, Xie WK, Hein TW, Kuo L, Rosa RH Jr. Laser-induced choroidal neovascularization in rats. *Methods Mol Biol* 2021;2319: 77-85.

5 Graham KW, Chakravarthy U, Hogg RE, Muldrew KA, Young IS, Kee F. Identifying features of early and late age-related macular degeneration: a comparison of multicolor versus traditional color fundus photography. *Retina* 2018;38(9):1751-1758.

6 Smith CA, Hooper ML, Chauhan BC. Optical coherence tomography angiography in mice: quantitative analysis after experimental models of retinal damage. *Invest Ophthalmol Vis Sci* 2019;60(5):1556-1565.

7 Nakagawa K, Yamada H, Mori H, Toyama K, Takahashi K. Comparison between optical coherence tomography angiography and immunolabeling for evaluation of laser-induced choroidal neovascularization. *PLoS One* 2018;13(8):e0201958.

8 Liang IC, Ko WC, Hsu YJ, Lin YR, Chang YH, Zong XH, Lai PC, Chang DC, Hung CF. The anti-inflammatory effect of hydrogen gas inhalation and its influence on laser-induced choroidal neovascularization in a mouse model of neovascular age-related macular degeneration. *Int J Mol Sci* 2021;22(21):12049.

9 Comin CH, Tsirukis DI, Sun Y, Xu XY. Quantification of retinal blood leakage in fundus fluorescein angiography in a retinal angiogenesis model. *Sci Rep* 2021;11(1):19903.

10 Zhang YF, Jiang C, Zhou XH, Wei DY, Li SH, Long P, Li MH, Zhang ZM, Chen T, Du HJ. Therapeutic effect of a traditional Chinese medicine formulation on experimental choroidal neovascularization in mouse. *Int J Ophthalmol* 2021;14(10):1492-1500.

11 Spaide RF, Klancnik JM Jr, Cooney MJ. Retinal vascular layers imaged by fluorescein angiography and optical coherence tomography angiography. *JAMA Ophthalmol* 2015;133(1):45-50.

12 Jia YL, Bailey ST, Hwang TS, McClintic SM, Gao SS, Pennesi ME, Flaxel CJ, Lauer AK, Wilson DJ, Hornegger J, Fujimoto JG, Huang D. Quantitative optical coherence tomography angiography of vascular abnormalities in the living human eye. *Proc Natl Acad Sci U S A* 2015;112(18):E2395-E2402.

13 Greig EC, Duker JS, Waheed NK. A practical guide to optical coherence tomography angiography interpretation. *Int J Retina Vitreous* 2020;6(1):55.

14 Ben Moussa N, Georges A, Capuano V, Merle B, Souied EH, Querques G. MultiColor imaging in the evaluation of geographic atrophy due to age-related macular degeneration. *Br J Ophthalmol* 2015;99(6):842-847.

15 Yu SQ, Bellone D, Lee SE, Yannuzzi LA. Multimodal imaging in foveal red spot syndrome. *Retin Cases Brief Rep* 2015;9(2):97-101.

16 Kokona D, Ebneter A, Escher P, Zinkernagel MS. Colony-stimulating factor 1 receptor inhibition prevents disruption of the blood-retina barrier during chronic inflammation. *J Neuroinflammation* 2018;15(1):340.

17 Lozano DC, Twa MD. Development of a rat schematic eye from *in vivo* biometry and the correction of lateral magnification in SD-OCT imaging. *Invest Ophthalmol Vis Sci* 2013;54(9):6446-6455.

18 Parravano M, Borrelli E, Sacconi R, Costanzo E, Marchese A, Manca D, Varano M, Bandello F, Querques G. A comparison among different automatically segmented slabs to assess neovascular AMD using swept source OCT angiography. *Transl Vis Sci Technol* 2019;8(2):8.

19 Yoneya S, Komatsu Y, Mori K, Deguchi T, Saitoh T, Young-Duvall J. The improved image of indocyanine green angiography in young healthy volunteers. *Retina* 1998;18(1):30-36.

20 Azar G, Vasseur V, Lahoud C, Favard C, de Bats F, Cochereau I, Yachvitz A, Mauget-Faÿsse M. Polypoidal choroidal vasculopathy diagnosis and neovascular activity evaluation using optical coherence tomography angiography. *Biomed Res Int* 2021;2021:1637377.

21 Lupidi M, Schiavon S, Cerquaglia A, Fruttini D, Gujar R, Muzi A, Fiore T, Reibaldi M, Chhablani J, Cagini C. Real-world outcomes of

anti-VEGF therapy in treatment-naïve neovascular age-related macular degeneration diagnosed on OCT angiography: the REVEAL study. *Acta Ophthalmol* 2021:Epub ahead of print.

22 Więcławek W, Danch-Wierzchowska M, Rudzki M, Sędziak-Marcinek B, Teper SJ. Ultra-widefield fluorescein angiography image brightness compensation based on geometrical features. *Sensors* (*Basel*) 2021;22(1):12.

23 Weinhaus RS, Burke JM, Delori FC, Snodderly DM. Comparison of fluorescein angiography with microvascular anatomy of macaque retinas. *Exp Eye Res* 1995;61(1):1-16.

24 Koustenis A Jr, Harris A, Gross J, Januleviciene I, Shah A, Siesky B. Optical coherence tomography angiography: an overview of the technology and an assessment of applications for clinical research. *Br J Ophthalmol* 2017;101(1):16-20.

25 Alnawaiseh M, Rosentreter A, Hillmann A, Alex AF, Niekämper D, Heiduschka P, Pap T, Eter N. OCT angiography in the mouse: a novel evaluation method for vascular pathologies of the mouse retina. *Exp Eye Res* 2016;145:417-423.

26 Liu L, Gao SS, Bailey ST, Huang D, Li DW, Jia YL. Automated choroidal neovascularization detection algorithm for optical coherence tomography angiography. *Biomed Opt Express* 2015;6(9):3564-3576.

27 Spaide RF, Fujimoto JG, Waheed NK. Image artifacts in optical coherence tomography angiography. *Retina* 2015;35(11):2163-2180.

28 Muftuoglu IK, Gaber R, Bartsch DU, Meshi A, Goldbaum M, Freeman WR. Comparison of conventional color fundus photography and multicolor imaging in choroidal or retinal lesions. *Graefes Arch Clin Exp Ophthalmol* 2018;256(4):643-649.

29 Pang CE, Freund KB. Ghost maculopathy: an artifact on near-infrared reflectance and MultiColor imaging masquerading as chorioretinal pathology. *Am J Ophthalmol* 2014;158(1):171-178.e2.

30 Alten F, Clemens CR, Heiduschka P, Eter N. Characterisation of reticular pseudodrusen and their central target aspect in multi-spectral, confocal scanning laser ophthalmoscopy. *Graefes Arch Clin Exp Ophthalmol* 2014;252(5):715-721.